Preparation and Thermal and Thermo-Oxidative Stability of Vinylidene Chloride-*co*-Vinyl Chloride Copolymer/ Synthetic Hectorite Nanocomposites

Tar-Hwa Hsieh,[1] Ko-Shan Ho,[1] Hsiaotao T. Bi,[2] Jan-Kuan Hung,[1] Yu-Kai Han,[1] Shin-Shiao Yang,[1] Yu-Chen Chang[3]

[1]*Department of Chemical and Materials Engineering, National Kaohsiung University of Applied Sciences, Kaohsiung 807, Taiwan*
[2]*Department of Chemical and Biological Engineering, University of British Columbia, Vancouver, BC V6T 1Z3, Canada*
[3]*Institute of Materials Science and Engineering, National Sun Yat-Sen University, Kaohsiung, Taiwan*

Received 7 August 2008; accepted 15 December 2008
DOI 10.1002/app.29916
Published online 7 May 2009 in Wiley InterScience (www.interscience.wiley.com).

ABSTRACT: Poly(vinylidene chloride-*co*-vinylchloride)/ organically modified hectorite (VDC-VC/SPN) nanocomposites were prepared by melt blending VDC-VC copolymer with SPN in the presence of dioctyl phthalate, which acted as a plasticizer. As a result, the exfoliated structure was found in the VDC-VC/SPN nanocomposites. In nitrogen atmosphere, VDC-VC/SPN nanocomposites exhibited a single-step thermal degradation. The thermal stability of VDC-VC/SPN nanocomposites is significantly influenced by the SPN, which was modified with long alkyl ternary ammonium salt. In air atmosphere, VDC-VC/SPN nanocomposites revealed a two-step thermo-oxidative degradation behavior. At the first degradation stage, the weight loss pattern is similar to that of VDC-VC composites in nitrogen, in which the thermo-oxidative stability of VDC-VC/SPN nanocomposites is affected by the ternary ammonium salt and oxygen rather than its morphology. At the second degradation stage, both the enhanced thermo-oxidative stability and the flame-retardation ability of VDC-VC composites are strongly and closely related to the morphology of nanocomposites. © 2009 Wiley Periodicals, Inc. J Appl Polym Sci 113: 3171–3180, 2009

Key words: poly(vinylidene chloride-*co*-vinyl chloride)/ organically modified hectorite nanocomposites; exfoliated nanostructure; thermal stability; thermo-oxidative stability; flame retardation

INTRODUCTION

Vinylidene chloride (VDC) polymer is a high-performance material because of its high crystallinity, high polarity and excellent gas barrier properties. However, discoloration, crosslinking, and reduction of the mechanical properties due to the poor thermal stability, which easily occurs when exposed to heat or light, turn out to be major problems for melt processing of the homo-poly(vinylidene chloride) (homo-PVDC). The current commercial success of VDC polymers depends on the use of copolymerization and plasticization to overcome the instability problem. The copolymers currently used in the commercial process, such as poly(vinylidene chloride-*co*-vinyl chloride) (VDC-VC copolymer), poly(vinylidene chloride-*co*-methyl acrylate) (VDC-MA copolymer) and poly(vinylidene chloride-*co*-acrylonitrile) (VDC-AN copolymer), are less crystalline, more soluble, and have lower melting temperatures and are thus easier to be processed than homo-PVDC. The most important application of those copolymers is as packing film to limit oxygen/water vapor transport.[1–3] However, new VDC copolymers with good gas barrier properties while maintaining other unique characteristics are still needed. The development of polymer-layered silicate nanocomposites (PLSNs) presents a new opportunity for the production of high-performance VDC copolymers for broadening packing material applications.

In the past decade, PLSNs have attracted intensive interest as barrier materials for a variety of packing applications.[4–7] Remarkable improvements on the gas barrier properties have been reported with the addition of low concentrations of layered silicate (<5 wt %) in polyimide,[8] polycaprolactone,[5] and poly(vinyl alcohol)[9] matrices. At the same time, mechanical, thermal, and flame-resistance properties were also simultaneously improved. Baroscopic dispersion of the layered silicate in a polymer matrix was found to result in a greater enhancement in gas barrier property compared with conventional phase-separated composites. However, less attention has been given to chlorinated polymers, especially VDC

Correspondence to: T.-H. Hsieh (thh@cc.kuas.edu.tw).

copolymers. Early work of Ishida et al.[10] suggested a novel approach for nanocomposites preparation where PVC was blended with a tin stabilizer in the presence of clay and epoxy with a spatula or a mortar, with only wide-angle X-ray diffraction test results being reported in their work. Trlica et al.[11] took dioctylphtalate (DOP) as co-intercalater for organic montmorillonite (organic-MMT) and PVC due to the presence of alkyl ammonium salt between the interlayers of organic-MMT, which can accelerate PVC degradation reaction. They found DOP prevented the degradation of PVC, and the MMT only acted as a plasticizer carrier with no significant enhancement on the mechanical properties of the composites. Wang et al.[12] further prepared highly intercalated PVC/organic-MMT nanocomposites by the melt intercalate technique and studied the thermal and mechanical properties of the nanocomposites in both the presence and the absence of DOP. Wang suggested that DOP acted as a plasticizer and co-intercalater for PVC and its composites. The organic-MMT can serve as a plasticizer for PVC in the absence of DOP. Both studies[11,12] indicate that the ternary ammonium salt-treated MMT played an important role in inducing the degradation of PVC. Chen et al.[13,14] prepared PVC/Na^+-MMT and PVC/organic-MMT nanocomposites by the melt-blending technique and investigated the thermal and mechanical properties of the nanocomposites in the absence of DOP. They found that partially encapsulated and intercalated structures formed in PVC/Na^+-MMT nanocomposites, while partially intercalated and partially exfoliated structures coexisted in PVC/organic-MMT nanocomposities. Both Na^+-MMT and organic-MMT can enhance the mechanical properties of PVC by the addition of a small amount of MMT (<3 phr) due to thermal instability. Recently, Kim and White[15] further extended the investigation of PVC composites to other chlorinated polymers [i.e., polychloroprene, chlorinated polyethylene, chlorinated-poly(vinyl chloride), and poly(vinylidene chloride) (PVDC)/clay nanocomposites], where chlorinated polymers were blended with natural MMT and ternary ammonium salt-treated MMT by using a Brabender operated at 180°C and 100 rpm, for various time intervals. They showed that natural MMT did not disperse well in chlorinated polymers, whereas organic-MMT dispersed well in chlorinated polymers and formed intercalated nanocomposites due to their polarity characteristics, showing enhanced tensile strength and Young's modulus of all the chlorinated polymers. Despite that, Kim and White have studied the characteristics of PVDC/organic-MMT nanocomposites; only morphology and mechanical properties data have been reported. The effect of clay on the thermal or thermo-oxidative stability of PVDC or VDC copolymers composites has not been investigated.

TABLE I
Element Analysis of the Commercial VDC-VC Copolymer

		C (%)	H (%)	Cl (%)
$(CH_2CCl_2)_X(CH_2CHCl)_{1-X}$	Calc.	26.63	2.44	70.94
	Found	26.59	2.51	70.90

As mentioned above, organic-MMT has been successfully applied as clay for the preparation of polymer/organic-clay nanocomposites and exhibited remarkable improvement in physical and chemical properties of the nanocomposites. However, it can also induce the degradation of chlorinated polymers, limiting the use of organic-MMT as clay for the preparation of chlorinated polymers hybrids. As reported in our previous study,[16] we successfully prepared VDC-VC copolymer/synthetic mica (MEE) (VDC-VC/MEE) nanocomposites by using melt blending method, with the composites exhibiting partially intercalated and partially exfoliated structures. In nitrogen atmosphere, the thermal stability of VDC-VC/MEE nanocomposites is strongly related to the morphology of nanocomposites and the degraded composites structure. Because synthetic hectorite has small dimensions and high polar surfactant, the complete absence of Fe ion impurities allows for the production of a composite, which is optically clear and completely colorless.[17] It may be an attractive candidate for the preparation of high-performance VDC copolymers for packing material applications.

In the present study, we mainly investigated the effect of synthetic hectorite on the nanostructure development and thermal stability of the VDC-VC/SPN composites. The VDC-VC/SPN composites were prepared by melt blending, in which VDC-VC copolymer containing 15 wt % DOP was used as the pristine polymer matrix. Effects of SPN content on the morphology and thermal and thermo-oxidative stability of VDC-VC composites were also studied.

MATERIALS AND METHODS

Materials

Commercial VDC-VC copolymer containing an acetyltributyl citrate (ACT) stabilizer of 4.07 wt % was acquired from Aldrich Chemical (USA). The VDC-VC copolymer was first purified with tetrahydrofuran (THF) (Echo Chemical Co., Ltd., Miao-Li, Taiwan), followed by the addition of ethanol, with the white powders of VDC-VC copolymer being separated by filtration. The obtained VDC-VC copolymer powder was characterized by elementary analysis (EA) by using Heraeus CHN-rapid and Tacussel Coulomax 78, with the results given in Table I

(Heralous Ltd., Hanau, Germany). According to EA results and follow-up calculation, the mole percentage of VDC monomer in VDC-VC copolymers is found to be about 80%.

The synthetic hectorite (Lucentite SPN) was provided by CO-OP Chemical Co., Ltd. (Tokyo, Japan). The SPN was modified by replacing Na^+ ions (cation exchange capacity of 101 mequiv/100 g, thickness ca. 1 nm, average length 50–60 nm) with poly(oxypropylene) methyl diethyl ammonium chloride ion $[(C_2H_5)_2(CH_3)N^+(O\text{-}iPr)_{25}]Cl^-$ by the ion exchange method. The VDC-VC copolymer processing additives, such as the stabilizer (ACT) and plasticizer (DOP), were all industrial grade products, and all materials were used as received.

Preparation of VDC-VC/SPN nanocomposites

SPN was first premixed with 15 wt % of DOP and placed in an ultrasonic bath at room temperature for 4 h. VDC-VC composites were then prepared by melt blending VDC-VC copolymer with SPN/DOP in a Brabender mixer at 160°C and 60 rpm, for various intervals of time. In the present work, the VDC-VC composites are designated as PVDC-DOP-SPN (e.g., PVDC-15-0 means containing15 wt % DOP and 0 wt % SPN).

UV–visible analysis

The UV–visible spectra were recorded at 300 nm/min scanning rate with regular intervals by using a U-2000 Hitachi UV–vis spectrophotometer. Solutions of the samples were prepared in distilled THF (7.5 g/L) in an ultrasonic bath at 50°C for 4 h and analyzed immediately.

Wide-angle X-ray diffraction

The powder X-ray diffraction patterns of the samples were obtained with a Rugaku Denki D/max-2200 diffractometer operated at 40 kV and 30 mA by using Cu Kα radiation ($\lambda = 0.154$ nm), with the diffraction angles (2θ) ranging from 2° to 30° at a scan rate of 1°/min.

Transmission electron microscopy

Samples were embedded in the epoxy resin and sectioned about 70 nm in thickness by using a Reichert microtone at room temperature. Samples were then corrected in a trough filled with methanol and placed on a 200-mesh copper grid for the transmission electron micrograph (TEM) observation. The TEMs were obtained with a Hitachi HF-2000 apparatus running at an acceleration voltage of 200 kV.

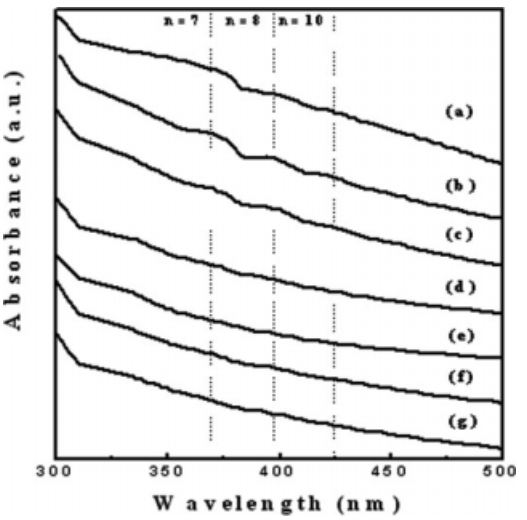

Figure 1 UV–vis spectra of VDC-VC copolymer with different DOP contents mixed at 160°C and 60 rpm for 5 min: (a) PVDC-0-0; (b) PVDC-5-0; (c) PVDC-10-0; (d) PVDC-12.5-0; (e) PVDC-15-0; (f) PVDC-17.5-0; (g) PVDC-20-0.

Thermogravimetric analysis

About 4–8 mg of samples was conducted in a DuPont SDT-2920 thermogravimetric analysis (TGA) unit at a heating rate of 10°C/min under a nitrogen and air atmosphere. The temperature scan ranged from room temperature to 700°C.

Limiting oxygen index

The limiting oxygen index (LOI) values were measured on a Dynisco Rev. 1.0 instrument. The percentage in the O_2–N_2 mixture deemed sufficient to sustain the flame was taken as the LOI value. The LOI values of VDC-VC/SPN composites were measured following ASTM standard D 2863-77 method. The dimensions of the samples used for the test were $100 \times 6.5 \times 3$ mm^3.

RESULTS AND DISCUSSION

UV–vis absorption spectra of VDC-VC copolymers prepared at 160°C for 5 min with different DOP contents are given in Figure 1. Below 10 wt % DOP, the UV–vis absorption spectra of the plasticized VDC-VC copolymer are found to demonstrate three absorption peaks at approximately $\lambda_{1max} = 369$ nm, $\lambda_{2max} = 397$ nm, and $\lambda_{3max} = 424$ nm, corresponding to the different numbers of conjugated double polyene bonds (n) of 7, 8, and 10, respectively.[18] The n value of VDC-VC copolymers significantly decreased with increasing DOP, indicating that the dehydrochlorination of VDC-VC copolymers was enhanced at lower DOP. It implies that the dehydrochlorination of VDC-VC copolymers can occur easily in the

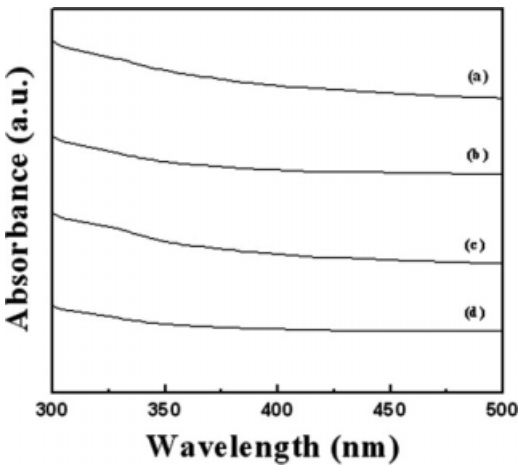

Figure 2 UV–vis spectra of VDC-VC/SPN composites: (a) PVDC-15-0; (b) PVDC-15-3; (c) PVDC-15-5; (d) PVDC-15-8. Samples mixed at 160°C and 60 rpm for 5 min.

absence of DOP. With DOP contents higher than 12.5 wt %, no absorption peaks ranged from 300 to 500 nm can be observed, indicating that VDC-VC copolymer did not degrade at higher DOP.[19] Figure 2 shows UV–vis absorption spectra of the composites prepared at 160°C for 5 min by mixing VDC-VC with different percentages of SPN. It is clearly seen that no absorption peaks from 300 to 500 nm can be observed, suggesting that the thermal degradation of VDC-VC/SPN composites is inherently independent of SPN and that VDC-VC/SPN composites may not be degraded during mixing and blending. In the present study, VDC-VC copolymer containing 15 wt % DOP was received and used as the VDC-VC matrix, and the effect of thermal degradation on the structure of VDC-VC/SPN composites during the mixing and compounding was neglected.

Morphology of VDC-VC/SPN nanocomposites

Figure 3 shows the X-ray diffraction patterns of VDC-VC/SPN composites prepared by mixing at 160°C for 5 min with different SPN contents. It can be seen that the characteristic (001) diffraction peak for SPN is located at approximately $2\theta = 2.30°$, corresponding to a basal spacing of 38.4 Å. As observed from Figure 3(b,c) (PVDC-0-5 SPN and PVDC-15-5 SPN), the basal spacing of the SPN disappears completely in the range of $2\theta = 1°$–$10°$, suggesting that either with or without the DOP, layered SPN were delaminated into disordered monolayers dispersed within the VDC-VC matrix and became a morphology of exfoliation. It suggests that DOP in the VDC-VC/SPN composites acts as a plasticizer to separate the SPN layers, leading to the development of exfoliated nanostructures. For DOP-free composites, SPN may act as a plasticizer itself and promote the

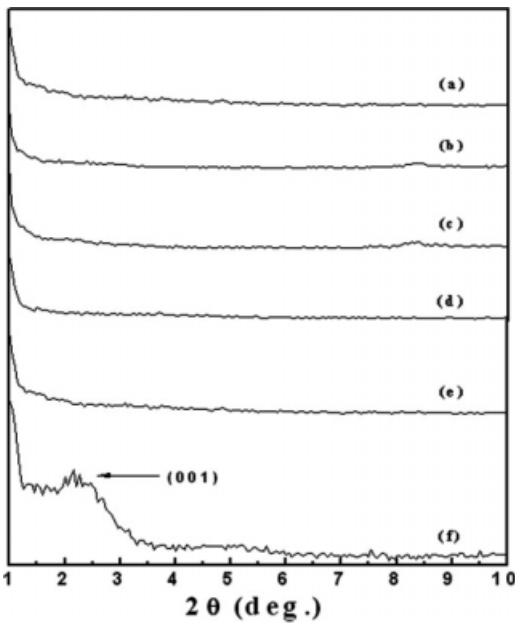

Figure 3 XRD patterns of VDC-VC composites with various SPN contents: (a) PVDC-15-0; (b) PVDC-15-3; (c) PVDC-15-5; (d) PVDC-15-8; (e) PVDC-15-0; (f) SPN.

formation of exfoliated nanostructures, resulted from the polar–polar interaction between VDC-VC and SPN layers. Similar results were reported by Ishida et al. and Wang et al.[10,12] Figure 3(d–f) shows that no diffraction peak in the range of $2\theta = 1°$–$10°$ is detected for all VDC-VC/SPN composites as well, indicating that none of the VDC-VC/SPN nanocomposites owned large-size ordered structures and that the clay gallery has been well expanded or destroyed by the VDC-VC copolymers. Typical TEM photographs of VDC-VC/SPN nanocomposites prepared by mixing with 15 wt % DOP and 5 wt % SPN at 160°C for 5 min is shown in Figure 4, where TEM micrographs with smaller magnification

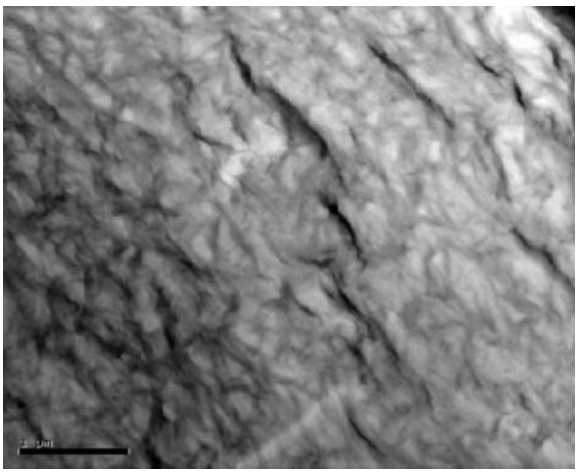

Figure 4 TEM micrographs of PVDC-15-5 composite with low magnification (×20,000).

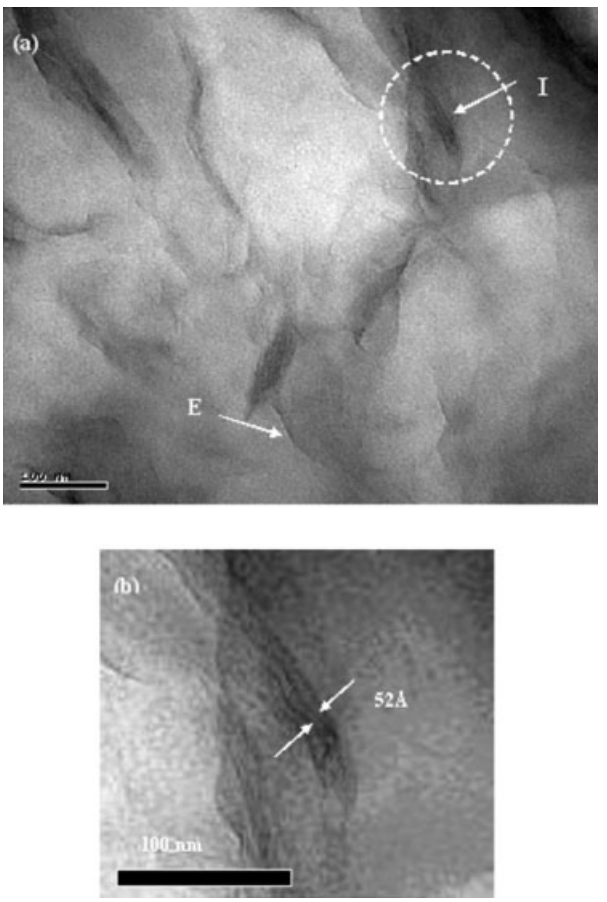

Figure 5 TEM micrographs of PVDC-15-5 composite with high magnification: (a) (×300,000); (b) the enlarged part (I) of the aggregative morphology.

demonstrate light and dark domains, corresponding to the VDC-VC and the layered SPN, respectively. It can be observed from Figure 4 that the SPN platelets are macroscopically dispersed within VDC-VC matrix. Figure 5(a) is the image of the same sample with higher magnification. The arrows (E) and (I) in the figure illustrate the exfoliated monolayer SPN platelets and the aggregative ones within VDC-VC matrixes, respectively. Figure 5(b) shows the enlarged part (I) of the aggregative domain, which reveals that the distance between delaminated SPN platelets is ca. 52 Å, which is significantly larger than the basal spacing of pristine SPN (d = 38.4 Å). It suggests that the SPN has been destroyed by the presence of VDC-VC copolymers. In combination with the wide-angle X-ray diffraction results in Figure 3, we found the partially ordered, partially exfoliated morphologies of VDC-VC/SPN nanocomposites due to melt mixing. The result suggests that the smaller aspect ratio of the SPN platelets provides less steric hindrance to allow the SPN platelets to disperse or aggregate more easily in the VDC-VC matrix. Furthermore, the presence of the slightly polar nature of the alkyl ammonium salt in SPN may

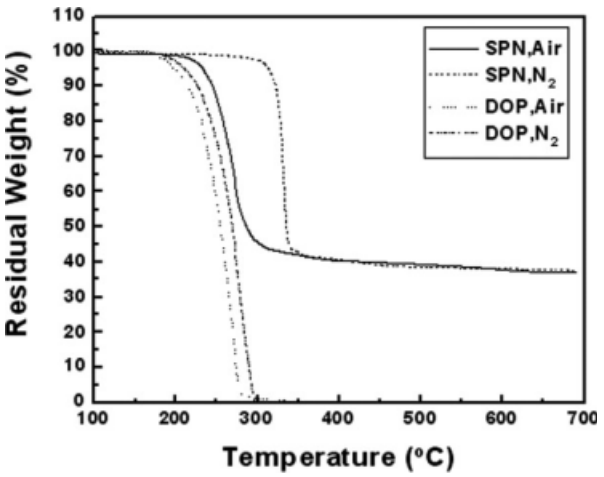

Figure 6 TGA thermograms of DOP and SPN under nitrogen and air atmospheres.

also improve the interaction between SPN platelets and the VDC-VC chains to result in the exfoliation.[17]

Thermal degradation

TGA thermograms for neat DOP and SPN obtained under nitrogen atmosphere are shown in Figure 6. It can be seen that the weight loss of the volatile DOP starts at ~200°C and nears 100% when the temperature is close to 300°C. Moreover, neat SPN exhibits one-step weight loss behavior in the range of 300–350°C. The weight loss of SPN begins at ~320°C due to the thermal decomposition of alkyl ammonium salt between silicate layers[20] and ca. 37% clay remained at 700°C. Similar results have been reported by Si and coworkers.[17] TGA-DTG (derivative thermogravimetry) thermograms for VDC-VC composites taken under a nitrogen stream are shown in Figure 7. It can be seen that VDC-VC composites follow a one-step thermal degradation process in the

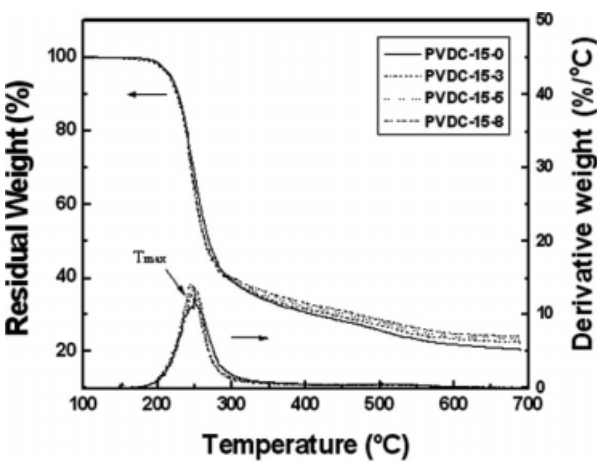

Figure 7 TGA-DTG thermograms of VDC-VC composites under nitrogen atmosphere.

range of 200–300°C without significant weight loss being detected when the temperature is below 190°C due to its slow degradation rate and the existence of an induction period for dehydrochlorination.[21] Hydrochloric gas is believed to be the main product gas from decomposition at temperatures below 190°C.[22,23] Although there is no significant weight loss, dehydrochlorination results in the production of an unsaturated structure of polyene in the backbones, which can trigger more complex degradation reactions. When the temperature is higher than the melting point, T_m (ca. 152°C, which is obtained from the DTA thermogram to be described later), the VDC-VC/SPN composites undergo two significant weight loss steps. The first one occurs in the range of 190–300°C, involving the loss of DOP and alkyl ammonium salt between silicate layers and a significant evaporation of the depolymerized VDC monomer. As a result, benzene, monochlorobenzene, *m*-dichlorobenzene, and 1,3,5-trichlorobenzene are produced in sequence followed by chain scission and cyclization, respectively.[24] The dehydrochlorization of the VC part is very rapid at high temperatures and stable double bonds form easily, which consequently stabilizes the neighboring VDC parts, making it difficult for VDC to undergo further chain scission reactions to release more VDC monomers.[25] As a consequence, the copolymer with a high content of VDC (as the received VDC-VC copolymer with a VDC mole fraction of 0.80) will yield a large amount of VDC monomer and 1,3,5-trichlorobenzene, as compared with benzene and its derivatives, although the relative yield of these materials depends on the VDC-VC conformation and VDC content.[25] At this stage, the degree of weight loss of VDC-VC matrix is significantly smaller than those of VDC-VC/SPN composites, suggesting that the organic modified hectorite plays an important role on inducing the degradation of VDC-VC composites in the presence of alkyl ammonium salt,[11,12] and hence, exhibiting poor thermal stability. For VDC-VC/SPN composites, the weight loss slightly increases with increasing SPN, which means that the induction effect of degradation can be enhanced at higher alkyl ammonium salt concentrations. As observed from DTG thermograms, the temperature corresponding to the maximum rate of weight loss (T_{max}) of VDC-VC matrix ca. 265°C is higher than that of VDC-VC/SPN nanocomposites (around ca. 250°C) due to the degradation-induction effect of alkyl ammonium salt, which leads to the earlier thermal degradation of VDC-VC/SPN. For VDC-VC/SPN nanocomposites, T_{max} value decreases, while the maximum rate increases with increasing SPN, revealing that the thermal degradation is significantly influenced by SPN content. However, the degree of SPN increases with increasing temperature and shows a strong relationship with the alkyl ammonium salt concentration rather than nanostructure. The result suggests that the exfoliated structure in VDC-VC/SPN nanocomposites may not be able to effectively stop the volatile gas evaporation from the composite at such a high dehydrochlorination rate, and hence, result in a poor thermal stability.

The second stage of weight loss occurs at temperatures higher than 300°C (at a residual weight of about 40%), in which the weight loss continues steadily at a relatively slow pace due to the slow release rate of volatile gases from the fully developed densely crosslinked structure resulting from intermolecular crosslinking of the unsaturated polymer chains.[24] However, this barrier effect is vanished at ca. 350°C due to the breakdown of the crosslinked network.[26] Compared to the VDC-VC composites, VDC-VC/SPN nanocomposites have less weight loss than the VDC-VC matrix, which means that the nanostructure of VDC-VC/SPN can effectively prevent the release of volatile gases, and hence, enhance its thermal stability. It demonstrates that the introduction of SPN may induce strong interactions between polar VDC-VC chains and SPN layers, leading to the easy formation of the exfoliated nanostructures. Because the exfoliation and dispersion of silicate layers lengthen the diffusion path of the evolved gas through the VDC-VC matrix, the improved thermal stability can be attributed to the better barrier effect of the clay layers.[27] For VDC-VC/SPN composites, the degree of weight loss decreases with the increase in the SPN content, suggesting that the barrier effect in the nanostructure will be significantly enhanced with increasing SPN. However, the degree of weight loss at this stage increases with increasing temperature and shows a strong relationship with the nanostructure rather than the crosslinked structure of the composite.

DTA thermograms for VDC-VC composites obtained under nitrogen atmosphere are shown in Figure 8. The melting point of all VDC-VC composites is about 152°C, with no observable difference for different types of VDC-VC composites. It is worth noting that there exists a distinct broad peak at around 260°C, which corresponds to the intermolecular crosslinking of the unsaturated polymer chains. The comparison of different VDC-VC composites in the figure shows that the peak temperature of crosslinking (T_c) of VDC-VC/SPN nanocomposites is 7–12°C lower than the neat VDC-VC (T_c is ca. 263.5°C). Significantly lower T_c values of VDC-VC/SPN nanocomposites can be attributed to the induction effect of alkyl ammonium salt in the nanocomposite, leading to the earlier occurrence of the crosslinking reaction. Figure 8 also displays an apparently endothermic peak at around 350°C, which

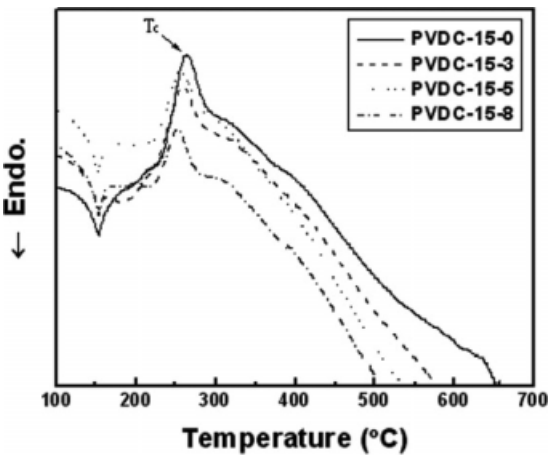

Figure 8 DTA thermograms of VDC-VC composites under nitrogen atmosphere.

corresponds to the breakdown of the crosslinked network.[25]

TGA data of VDC-VC composites obtained under nitrogen stream are summarized in Table II, where $T_{10\%}$, X_{rel}, char yield (%), and polymeric char yield (%) represent the temperature at which 10% degradation occurs, the relative degree of the crosslinking (the integration of the DTA peak per unit mass of VDC-VC/SPN composite relative to the VDC-VC matrix), the fraction of nonvolatile at 700°C, and the net char yield at 700°C with the residual SPN content after subtraction, respectively. It can be seen that $T_{10\%}$ values of VDC-VC/SPN nanocomposites are lower than that of neat VDC-VC due to the induction effect. The $T_{10\%}$ value of VDC-VC/SPN nanocomposites slightly decreases as the SPN content increases, suggesting that the weight loss at 10% degradation is dependent on the alkyl ammonium salt concentration. It is also worth noted that at higher SPN contents, T_c and X_{rel} values of VDC-VC/SPN nanocomposites are lower than the VDC-VC matrix, which can be attributed to the induction effect of ternary ammonium salt. The intermolecular crosslinking reaction occurs at a lower temperature, leading to the partially developed crosslinked network structure and lower X_{rel} value. Table II also shows that VDC-VC/SPN nanocomposites have higher char yield than VDC-VC matrix, suggesting that the VDC-VC/SPN nanocomposites exhibit better thermal stability due to its nanostructured morphology. For the VDC-VC/SPN system, the polymeric char yield increases by increasing the SPN. The SPN in the nanocomposites involved in the formation of a heat-resistant char serves as a superior insulator and mass transport barrier to the volatile products generated during decomposition.[28] It is reasonable to infer that the increase in the fraction of SPN can increase the amount of polymeric char to decrease the release of the volatile products. It suggests that the thermal stability of VDC-VC/SPN nanocomposites was improved at higher temperatures with the high char yields. Besides the barrier effect in the nanocomposites, another possible explanation is that DOP serves to separate the SPN layers, leading to the fully developed and densely crosslinked structure by intermolecular crosslinking of the unsaturated polymer chains.

Thermo-oxidative degradation and flame retardation

As observed from Figure 6, the weight loss behavior of DOP in air is similar to that in nitrogen. Moreover, SPN exhibits the one-step weight loss in the temperature range of 200–300°C, in which the weight loss starts at ca. 220°C with ca. 37% clay still remaining at 700°C. Figure 9 shows the TGA-DTG thermograms of VDC-VC composites under air atmosphere. It can be observed that VDC-VC composites follow a two-step thermo-oxidative degradation in the temperature range of 200–300 and 450–650°C, respectively. Figure 10 displays the TGA thermograms of VDC-VC composites under nitrogen and air atmospheres, respectively. It can be seen that before the breakdown of crosslinked structure

TABLE II
TGA Data of VDC-VC Composites Under Nitrogen Atmosphere

Sample	$T_{10\%}$ (°C)	T_c (°C)	T_{max1}[a] (°C)	X_{rel}[b]	Char yield (%)[c]	Polymeric char yield (%)[c]
SPN	322.5	–	–	–	37.69	–
PVDC-15-0	227.6	263.5	264.8	1.00	20.48	20.48
PVDC-15-3	226.1	256.7	250.4	0.94	22.31	21.18
PVDC-15-5	225.1	256.2	250.2	0.90	23.14	21.26
PVDC-15-8	224.8	251.7	244.7	0.82	24.12	21.10

[a] Peak temperature of maximum rate in DGT thermogram.
[b] Integration of the DTA peak per unit mass of VDC-VC/SPN composite relative to the VDC-VC matrix.
[c] Obtained at 700°C.

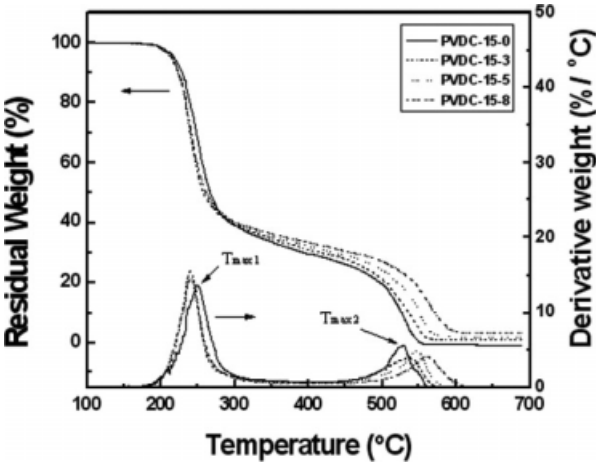

Figure 9 TGA-DTG thermograms of VDC-VC composites under air atmosphere.

(ca. 350°C), the thermo-oxidative degradation behavior of VDC-VC composites in air is similar to that in nitrogen, and the similar thermal degradation behavior can be significantly extended to ca. 400°C with the introduction of SPN (i.e., PVDC-15-5), which is likely contributed from the presence of the nanostructure. The weight loss occurs in this temperature range, involving hydrochloric gas, VDC monomer, aldehydic, ketonic, and aromatic species as well as some of their oxidized species (i.e., carboxylic acid, cyclic anhydrides, and lactonic) produced in sequence followed by chain scission and cyclization, respectively.[24] However, the relative yield of the released materials is dependent on VDC-VC conformation, VDC content, and the oxygen concentration in the atmosphere.[25,29] At temperatures higher than 450°C, it is noted that the sample weight deceases sharply with the increasing temperature, followed by almost 100% weight loss at about 600°C, suggesting that the VDC-VC composites start burning in air at ca. 475°C and are burned out near 600°C.[29] Polyaromatic species is believed to be the main gas product for VDC-VC composites decomposing in air stream in this temperature range,[29] and due to its nanostructure, the weight loss of VDC-VC/SPN nanocomposites is significantly lower than the VDC-VC matrix. For VDC-VC/SPN composites, the degree of weight loss decreases remarkably with the increase in the SPN, indicating that the retardation effect in thermo-oxidative degradation comes from the enhanced barrier effect with higher SPN contents. As observed from DTG thermograms, the T_{max1} of VDC-VC matrix ca. 256°C is higher than the VDC-VC/SPN nanocomposites (around ca. 245°C) due to the induced effect from the ternary ammonium salt, which leads to the occurrence of thermo-oxidative degradation at lower temperatures. For VDC-VC/SPN nanocomposites, the T_{max1} value decreases while the maximum rate increases with increasing SPN content, indicating that the thermo-oxidative degradation is significantly affected by the SPN content. However, the degree of weight loss increases with increasing temperature and shows a strong relationship with the concentration of alkyl ammonium salt rather than its nanostructure. When compared to Figure 7, it is noted that values of T_{max1} and the maximum rate (R_{max1}) of VDC-VC composites in air are significantly lower than that in nitrogen, suggesting that oxygen in the atmosphere acts as a catalyst to accelerate the rate of dehydrochlorination of VDC-VC composites.[30] Moreover, the T_{max2} of VDC-VC matrix is ca. 7–35°C, significantly lower than VDC-VC/SPN nanocomposites due to the barrier effect of the nanocomposite, which leads to the occurrence of combustion at lower temperatures. For VDC-VC/SPN nanocomposites, the T_{max2} value increases while the maximum rate (R_{max2}) decreases with the increase in the SPN content, indicating that the combustion behavior is significantly dependent on the SPN content.

DTA thermograms for VDC-VC composites obtained under air atmosphere are shown in Figure 11. It can be seen that the T_m of VDC-VC composites shows no observable difference for different VDC-VC composites. It is worth noting that the relatively small T_c peak, a distinct exothermic peak at around ca. 450–600°C, may correspond to the combustion peak of VDC-VC composites. The comparison of different VDC-VC composites in the figure shows that the peak temperature of combustion (T_{bp}) of VDC-VC/SPN nanocomposites is significantly ca. 35°C higher than the VDC-VC matrix. The relatively high T_{bp} value of VDC-VC/SPN nanocomposites can be attributed to the barrier effect with the reduced oxygen permeability in the nanocomposites, which leads to the significant

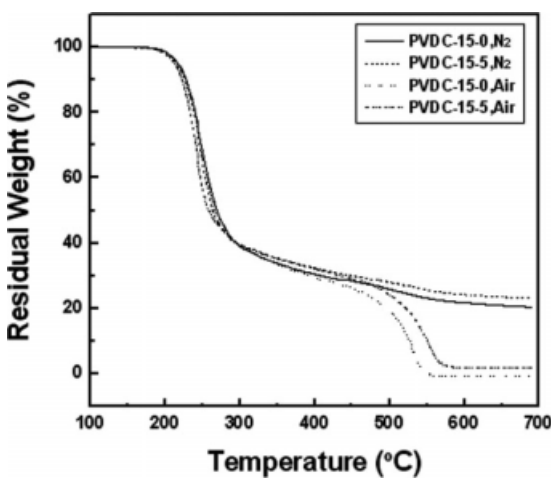

Figure 10 DTA thermograms of VDC-VC composites under nitrogen and air atmospheres.

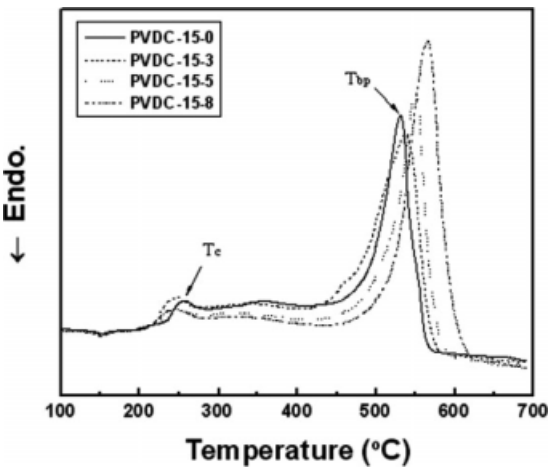

Figure 11 DTA thermograms of VDC-VC composites under air atmosphere.

retardation of the combustion reaction in the VDC-VC composites.

TGA data of VDC-VC composites obtained in the air stream are summarized in Table III, where Δ_2 weight (%, mg^{-1}), ΔH_{rel}, and LOI represent the integration of the second DTG peak per unit mass of sample, the relative combustion heat (sample weight multiplied by the integration area of the maximum exothermic peak in DTA thermogram to the VDC-VC matrix), and the limiting oxygen index, respectively, where ΔH_{rel} value may be related to the heat of combustion of VDC-VC composites if the heat capacity of the sample is assumed to be constant during the combustion process. It can be seen that $T_{10\%}$ values of VDC-VC/SPN nanocomposites are lower than the VDC-VC matrix due to the presence of the ternary ammonium salt, which can induce the thermal degradation. The $T_{10\%}$ value of VDC-VC/SPN nanocomposites slightly decreases with the increase in the SPN content, which means that the weight loss at 10% thermo-oxidative degradation is dependent on the concentration of the alkyl ammonium salt. It is worth noting that at higher SPN contents, T_c and X_{rel} values of VDC-VC/SPN nanocomposites are lower than the VDC-VC matrix, indicating the preoccurrence of the intermolecular crosslinking reaction of VDC-VC/SPN nanocomposites and the incomplete development of the crosslinked structure resulting from the induced effect of the ternary ammonium salt and catalytic effect from oxygen,[30] respectively. When compared with Table II, it is noted that, T_c and X_{rel} values of VDC-VC/SPN composites in air are significantly lower than the VDC-VC matrix in nitrogen, suggesting that the presence of oxygen can effectively accelerate the thermo-oxidative degradation, resulting in lower T_c and X_{rel} values of VDC-VC composites. Table III also shows that there is almost no polymeric char residue for VDC-VC/SPN nanocomposites, suggesting that the presence of oxygen can enhance dehydrochlorination, by partially oxidizing polyene chain, and, as a result, all char is completely oxidized with the resulting products volatilized.[30]

The Δ_2 weight of VDC-VC/SPN nanocomposites is seen to be lower than that of the VDC-VC matrix, while the polymeric char yield is higher than VDC-VC matrix, indicating that VDC-VC/SPN nanocomposites exhibit better thermo-oxidative stability due to the presence of the nanostructure. For the VDC-VC/SPN system, the polymeric char yield increases while the Δ_1 weight value decreases with increasing SPN content, indicating that the increase in the fraction of SPN increases the amount of polymeric char that can be formed to delay the release of the volatile products. This suggests that VDC-VC/SPN nanocomposites possess improved thermo-oxidative stability with higher T_{bp} and high char yields. Table III also shows that VDC-VC/SPN nanocomposites have higher ΔH_{rel} and LOI values than the VDC-VC matrix, indicating that the VDC-VC matrix becomes more difficult to be combusted as the SPN is introduced. The reduced values of ΔH_{rel} and LOI make VDC-VC/SPN nanocomposites better at flame

TABLE III
TGA and DTA Data of VDCVC Composites Under Air Atmosphere

Sample	$T_{10\%}$ (°C)	T_c (°C)	T_{max1} (°C)	X_{rel}	Δ_2 Weight[a] (% mg^{-1})	T_{bp}[b] (°C)	ΔH_{rel}[c]	Polymeric char yield[d] (%)	LOI
SPN	245.1	–	–	–	–	–	–	–	–
PVDC-15-0	227.6	256.1	249.8	1.00	5.7	530.9	1.00	0.00	35
PVDC-15-3	222.6	247.4	241.4	0.92	5.0	537.4	1.07	0.04	36
PVDC-15-5	220.1	246.2	240.2	0.85	4.8	549.9	1.22	0.07	37
PVDC-15-8	218.4	245.3	238.6	0.74	4.6	564.4	1.37	0.19	37

[a] Integration of the second DTG peak per unit mass of sample.
[b] Peak temperature of the thermo-oxidative degradation.
[c] VDC-VC/SPN sample weight multiplied by the integration area of the maximum exothermic peak in DTA thermogram to the VDC-VC matrix.
[d] Obtained at 700°C.

retardancy. For VDC-VC/SPN nanocomposites, the values of ΔH_{rel} and LOI increase with the increase in the SPN content, suggesting that the increased SPN content enhances the barrier effect and decreases the oxygen permeability, leading to enhanced flame retardation capability because of the reduced oxygen permeation. The result demonstrates that TGA data of VDC-VC composites obtained in air may well correspond to the thermo-oxidative stability or the flame retardancy of the composites.

CONCLUSIONS

VDC-VC/synthetic hectorite composites were prepared by melt blending of VDC-VC copolymer with SPN in the presence of DOP, which acted as a plasticizer. WADX and TEM results showed that the exfoliated structures existed in VDC-VC/SPN nanocomposites. For TGA analysis in nitrogen atmosphere, VDC-VC/SPN nanocomposites exhibited a single-step thermal degradation behavior, and the ternary ammonium salt-treated SPN played an important role in inducing the degradation of VDC-VC composites. In air atmosphere, VDC-VC/SPN nanocomposites showed a two-step thermo-oxidative degradation behavior. The weight loss behavior in the first stage of low temperature was similar to the VDC-VC composites in nitrogen. The thermo-oxidative stability was strongly dependent on the ternary ammonium salt and oxygen rather than on the nanostructure. In the second degradation stage at higher temperatures, the enhanced thermo-oxidative stability or flame retardancy of VDC-VC composites was strongly and closely related to the morphology of nanocomposites.

References

1. Wessling, R. A. In Polyvinylidene Chloride; Merz, E. M. Ed.; Gordon and Breach: New York, 1997; Chapter 6.
2. Schidknecht, C. E. In Vinyl and Related Polymers; Mark, H. Ed.; Wiley: New York, 1952; Chapter 8.
3. Wessling, R. A. In Encyclopedia of Polymer Science and Technology; Harman, F. M. Ed.; Wiley: New York, 1971; Vol. 14, p 540.
4. Drozdov, A. D.; Christiansen, J. D.; Gupta, R. K.; Shah, A. P. J Polym Sci Part B: Polym Phys 2003, 41, 476.
5. Messersmith, P. B.; Giannelis, E. P. J Polym Sci Part A: Polym Chem 1995, 33, 1047.
6. Gorrasi, G.; Tortora, M.; Vittoria, V.; Pollet, E.; Lepoittevin, B.; Alexandre, M.; Dubois, P. Polymer 2003, 44, 2271.
7. Osman, M. A.; Mittal, V.; Morbidelli, M.; Suter, U. W. Macromolecules 2003, 36, 9851.
8. Lu, J.; Ke, Y.; Qi, Z.; Yi, X. S. J Polym Sci Part B: Polym Phys 2001, 39, 115.
9. Ogata, N.; Kawakage, S.; Ogihara, T. J Appl Polym Sci 1997, 66, 573.
10. Ishida, H.; Campbell, S.; Blackwell, J. Chem Mater 2000, 12, 1260.
11. Trlica, J.; Kalendova, A.; Malac, Z.; Simonik, J. SPE ANTEC 2001, 1, 2162.
12. Wang, D.; Parlow, D.; Qlang, Y.; Wikie, C. A. J Vinyl Additive Technol 2001, 7, 203.
13. Chen, C. H.; Teng, C. C.; Yang, C. H. J Polym Sci Part B: Polym Phys 2005, 43, 1465.
14. Chen, C. H.; Teng, C. C.; Tsai, I. S.; Yen, F. S. J Polym Sci Part B: Polym Phys 2006, 44, 2145.
15. Kim, Y.; White, J. L. J Appl Polym Sci 2003, 90, 1581.
16. Hsieh, T. T.; Huang, J. K.; Ho, K. S.; Bi, S. S.; Chang, Y. C. J Polym Sci Part B: Polym Phys 2008, 46, 1214.
17. Si, M.; Goldman, M.; Rudomen, G.; Gelfer, M. Y.; Sokolov, J. C.; Rafailovich, M. H. Macromol Mater Eng 2006, 291, 602.
18. Abbås, K. B.; Laurence, R. L. J Polym Sci Part A: Polym Chem 1975, 13, 1889.
19. Dennis, H. R.; Hunter, D. L.; Chang, D.; Kim, S.; White, J. L.; Cho, J. W.; Paul, D. R. Polymer 2001, 42, 9513.
20. Xie, W.; Gao, Z.; Pan, W. P.; Hunter, D.; Singh, A.; Vaia, R. Chem Mater 2001, 13, 2979.
21. Hsieh, T. H.; Ho, K. S. J Polym Sci Part A: Polym Chem 1999, 37, 2035.
22. Hay, J. N. J Polym Sci A-1: Polym Chem 1970, 8, 1201.
23. Bohme, R. D.; Wessling, R. A. J Appl Polym Sci 1972, 16, 1761.
24. Chen, C. L.; Hsieh, T. H.; Ho, K. S. Polym J 2001, 33, 835.
25. Tsuge, S.; Okumoto, T.; Takeuchi, T. Die Makromol Chem 1969, 23, 123.
26. Mcneill, J. C.; Memetea, L.; Cole, W. J. Polym Degrad Stab 1995, 49, 181.
27. Golebiewski, J.; Galeski, A. Compos Sci Technol 2007, 67, 3442.
28. Gilman, J. W.; Jackson, C. L.; Morgan, A. B.; Harris, R., Jr.; Manias, E.; Giannelis, E. P.; Wuthenow, M.; Hilton, D.; Phillips, S. H. Chem Mater 2000, 12, 1866.
29. Oshea, H. L.; Morterra, C.; Low, M. J. D. Mater Chem Phys 1991, 27, 155.
30. Aracil, I.; Font, R.; Conesa, J. A. J Anal Appl Pyrol 2005, 74, 215.